Bull Earthquake Eng (2014) 12:1177–1200
DOI 10.1007/s10518-013-9554-0

ORIGINAL RESEARCH PAPER

Equivalent-linear stiffness and damping in rocking of circular and strip foundations

O. Adamidis · G. Gazetas · I. Anastasopoulos · Ch. Argyrou

Received: 17 February 2013 / Accepted: 7 November 2013 / Published online: 27 November 2013

Abstract An approximation is developed for obtaining the nonlinear stiffness K_R and damping C_R of a shallow circular or strip footing undergoing rocking oscillation on a homogeneous but inelastic undrained clayey stratum. Based on the parametric results of 3-D and 2-D finite-element analyses, equivalent-linear K_R and C_R are expressed in readily usable dimensionless forms. K_R, normalized by its linear elastic value, is shown to be a unique function of: (1) the vertical factor of safety F_s against static bearing capacity failure, and (2) the angle of rotation ϑ normalized by a characteristic angle ϑ_s. The latter is approximately the angle for which uplifting usually initiates at one edge of the foundation. Three sources contribute to the value of the dimensionless damping ratio ξ_R (derived from C_R): wave radiation, which is a function of frequency but is shown to amount to $<3\,\%$; soil inelasticity (hysteresis), for which graphs are developed in terms of ϑ/ϑ_s and F_s; and energy loss due to impact and the collateral vertical motion when severe uplifting takes place, which is tentatively determined from dynamic $M:\vartheta$ loops. Comparative parametric seismic time-history analyses provide an adequate validation of the iterative equivalent-linear approximation which implements the developed equivalent K_R and ξ_R, but they also highlight its limitations.

O. Adamidis, I. Anastasopoulos and Ch. Argyrou were formerly in the National Technical University, Athens, Greece.

O. Adamidis
University of Cambridge, Cambridge, UK

G. Gazetas (✉)
National Technical University, Athens, Greece
e-mail: gazetas@ath.forthnet.gr

I. Anastasopoulos
University of Dundee, Dundee, UK

Ch. Argyrou
Cornell University, Ithaca, NY, USA

Keywords Shallow foundations · Seismic response · Soil–structure interaction · Uplifting · Soil failure · Equivalent linear

1 Introduction

Subjected to strong seismic shaking, structures tend to experience large inertial forces. For tall-slender structures these forces will lead to overturning moments onto the foundation that may be disproportionally large compared to the vertical load. As a result, a shallow foundation may experience detachment (uplifting) of one edge from the supporting soil. This in turn will lead to increased normal stresses under the opposite edge of the foundation. Development of a bearing capacity failure mechanism is quite possible if such a concentration leads to sufficiently large stresses. But even then failure may not occur. Thanks to the *cyclic* and *kinematic* nature of earthquake induced vibrations: (1) the inertial forces do not act "*forever*" in the same direction to cause failure, but being cyclic, very soon reverse and thereby unload the distressed soil; and (2) the developing inertial forces are not externally applied and predetermined loads, but are themselves reduced once the soil-foundation system reaches its (limited) ultimate resistance. As a result, the system experiences nonlinear-inelastic rocking oscillations, which may or may not result in excessive settlement and rotation. Reference is made to a wealth of publications dealing with rocking–uplifting and overturning, and rocking–induced soil yielding and bearing capacity failure (Housner 1963; Meek 1975; Koh et al. 1986; Makris and Roussos 2000; Zhang and Makris 2001; Gazetas and Apostolou 2004; Gajan et al. 2005; Gerolymos et al. 2005; Apostolou et al. 2007; Gajan and Kutter 2008; Anastasopoulos 2010; Abate et al. 2010; Panagiotidou 2010; Pecker 2011; Massimino and Maugeri 2013).

A rigorous detailed analysis of soil–structure systems requires the use of advanced numerical tools with 3-D modeling of the ground and suitable complex constitutive relations for the soil. Although such analyses have been published in a number of research papers (e.g., Paolucci 1997; Paolucci and Pecker 1997; Kawashima et al. 2007; Anastasopoulos et al. 2010; Gelagoti et al. 2012; Kourkoulis et al. 2012; Panagiotidou et al. 2012) the task is hardly an easy one and would certainly not be justified for many engineering projects. Several attempts have thus been made to devise simple (or at least simpler) methods for computing the soil reaction to rocking. They include a variety of elastoplastic models with tensionless Winkler-type springs or a collection of springs-dashpots-sliders (Martin and Lam 2000; Allotey and El Naggar 2003; Chen and Lai 2003; Houlsby et al. 2005; Gerolymos and Gazetas 2006; Pitilakis et al. 2008; Harden et al. 2006; Apostolou 2011). Between these two approaches there is the development of comprehensive inelastic "macro-elements" which replace the soil by providing its force/moment reactions to footing displacements/rotations, in all modes of vibration (Cremer et al. 2002; Kutter et al. 2003; Paolucci et al. 2008; Chatzigogos et al. 2009; Figini 2010; Pecker 2011; Paolucci et al. 2013).

On the other hand, another simple idea emerged recently: nonlinearities of the soil-foundation system which develop during rocking could be handled approximately through a *simplified equivalent linear iterative visco-elastic approach*, *a* is done in wave propagation ("SHAKE") analyses using secant-modulus and damping curves, $G : \gamma$ and $\xi : \gamma$. To this end, Figini (2010) developed curves of effective stiffness, K_R, and effective damping, ξ_R, in terms of the angle of rotation and the vertical factor of safety against bearing-capacity failure. His curves were based primarily on available experimental data on dry sand: the large-scale cyclic tests of the European research program *TRISEE* (Faccioli et al. 1998). Recently, Gazetas et al. (2013) utilized theoretical results from nonlinear finite element analyses to develop a

dimensionless expression and an accompanying chart for the equivalent-linear *static stiffness* of various foundation shapes rocking on saturated undrained clay.

The work presented here extends the above work. It focuses mainly on developing *equivalent damping* in rocking of circular and strip foundations. A conceptual understanding of the physics of the problem guides the selection of the key dimensionless parameters. For completeness, expressions and charts for the dynamic stiffness are also summarized. The effectiveness of the developed approximations is then explored with a dynamic response analysis of a typical bridge-pier type structure–foundation under seismic excitation.

2 Problem statement

The studied problem is illustrated in Fig. 1a. Strip footings (plane-strain geometry) and circular footings (three-dimensional axisymmetric geometry) are examined. They rest on a soil stratum of saturated homogeneous clay which responds in undrained mode, with shear strength S_u and low-strain shear modulus G_o. Rigid bedrock underlies the clay. The footings are perfectly rigid.

Driven by seismic base excitation, a (simple) tall superstructure transmits onto the foundation (in addition to a shear force) a substantial overturning moment $M = M(t)$ that induces rocking oscillations. If M is large enough, the footing may uplift and the supporting soil may respond inelastically, eventually even mobilizing bearing-capacity failure mechanisms. Such mechanisms will last only "momentarily" and develop alternatingly under each edge of the footing; the final possible outcome being an accumulated settlement and a permanent rotation, or in some cases even complete overturning (driven by the combined inertia *and* gravity loads).

A crude sketch of an overturning moment-rotation curve, $M : \vartheta$, in Fig. 1c illustrates the definition of an effective rocking stiffness K_R and an effective *hysteretic* damping factor ξ_R. Being functions of the amplitude of the angle ϑ, these K_R and ξ_R are appropriate for (slow) cyclic loading. Under dynamic loading, stiffness and damping will in addition be functions of frequency. Moreover, damping is produced not only by hysteresis (inelastic action) but also by radiation and impact.

3 Numerical experiments: method of analysis and soil modelling

To develop nonlinear spring and dashpot, rigorous numerical (finite element) analyses are performed using ABAQUS and the parametric results are treated as our numerical experiments. Specifically, the analyses lead to graphs that display the decline of secant stiffness (K_R) and the increase of damping ratio (ξ_R) as the angle of rotation increases. Properly normalized to become independent of key dimensional parameters (such as soil shear strength S_u, soil shear modulus G, footing width B, and footing shape), these graphs form the basis of the equivalent linear approximation.

The soil is discretized into continuum solid 4-noded finite elements in plane-strain analyses, or continuum solid 8-noded elements in three dimensions. The mesh is thinly refined, with at least 12 elements under the width (or diameter) of the footing. Between foundation and soil we introduce an interface ("gap") element that allows detachment and sliding. However, a fairly substantial coefficient of friction ($\mu = 1.5$) is deliberately chosen, to prevent gross sliding. To achieve stable integrations we modified the default hard contact-pressure–over-closure relation in ABAQUS with a suitable exponential one.

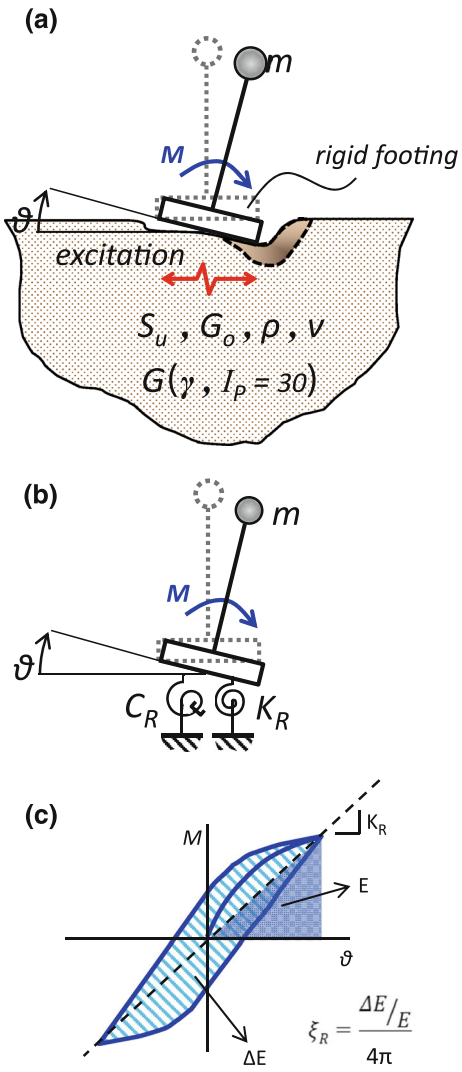

Fig. 1 Problem definition: **a** SDOF system on nonlinear undrained clay; **b** replacing the soil with equivalent-linear rotational spring and dashpot; **c** definition of secant stiffness and hysteretic damping factor from the monotonic and cyclic moment–rotation response curves

Different types of boundaries are used for static and seismic loading conditions as shown in Fig. 2. Static boundaries need only be placed well outside the "pressure bulb" and can be of any "elementary" type (from fixed to free). With *moment* static loading (monotonic or cyclic) on the surface of a homogeneous halfspace primarily normal vertical (+ and −) stresses are induced; they decay very rapidly in both the horizontal and vertical direction ("pressure bulb" less than one half-width from the foundation edge). Hence, the static boundaries could be safely placed at relatively small distances from the edges of the footing (total length L in Fig. 2). However, as is well known, under dynamic loading special "transmitting" boundaries must be placed at a suitably large distance to enable satisfactory wave propagation to infinity, and thereby to avoid spurious reflections that would undercut radiation damping. After a number of trials, the solution adopted here was an $L = 10\,B$, for the static problem, and placement of the so-called ABAQUS "infinite elements" at $L = 10\,B$ for the dynamic problem.

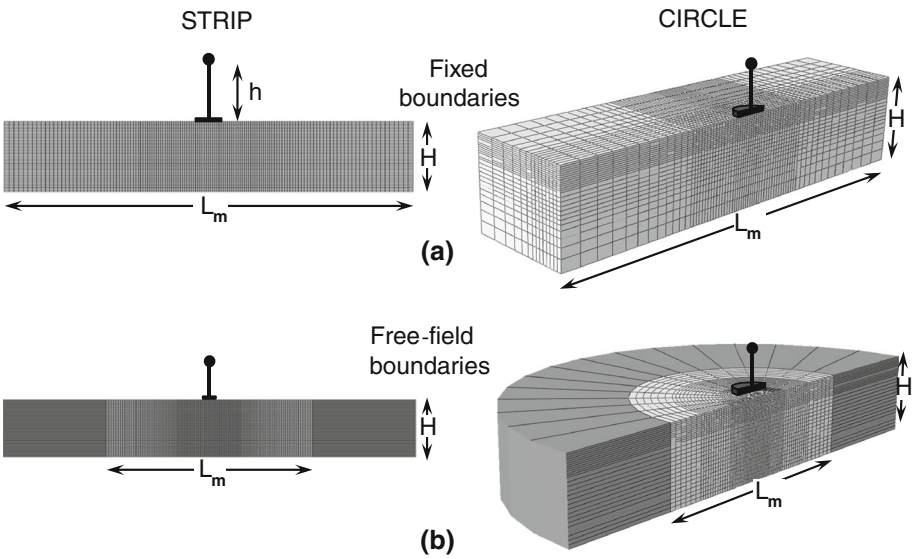

Fig. 2 Lateral boundaries used for the static and dynamic F.E. models: **a** fixedboundaries for static loading; **b** addition of "infinite" elements for the dynamic problems

Inelastic soil behavior under undrained conditions is described through a nonlinear kinematic hardening model with a Von Mises failure criterion and associative flow rule Description of the model requires, among others, determination of the (undrained) Young's elastic modulus E_u and shear strength S_u. The relevant parameters are calibrated by fitting the published $G : \gamma$ curve of Vucetic and Dobry (1991) for plasticity index $I_P = 30$. Further details on the constitutive relationship have been given by Anastasopoulos et al. (2010) and are not reproduced here.

To test the performance of the our model: (1) the computed static ultimate vertical forcing N_{uo} of a strip was compared successfully (error <5 %) with the classical analytical solution of Prandtl, $N_{uo} = (\pi + 2)S_u B$; (2) the static elastic stiffness of circular footing in vertical loading was verified (error $\approx +5\,\%$) against the closed-form solution $K_v = 4GR/(1 - \upsilon)$; and (3) the static elastic stiffness of strip footing of half width, b, in rocking was verified (error $\approx +10\,\%$) against the closed form solution $K_R = (\pi/2)Gb^2/(1 - \upsilon)$.

4 Equivalent-linear stiffness

4.1 Static stiffness

Equivalent stiffness in rocking $K_R = M/\vartheta$ is determined as the slope of the secant modulus of the appropriate $M - \vartheta$ monotonic response (pushover) curve. For a footing *bonded* onto a homogeneous *elastic* halfspace, K_R depends on the shear modulus G, the radius of the footing to the third power R^3 (or the width to the second power B^2 for plane conditions), and Poisson's ratio υ. However, when soil is a nonlinear inelastic material and separation of the footing from the supporting-ground surface cannot be inhibited, the value of undrained shear strength S_u, the vertical force N, and (most importantly) the angle of rotation ϑ, become decisive parameters. In addition, the effective shear modulus G becomes a function of the shear strain and the "plasticity" index:

$$G/G_o = \Gamma(\gamma; I_P) \tag{1}$$

By recourse to the Vaschy–Buckingham dimensional analysis (Palmer 2008), the following expression can be written for the ratio of $K_R/K_{R,elastic}$ as a function, f, of the problem dimensionless parameters:

$$\frac{K_R(\vartheta, N)}{K_{R,elastic}} = f\left(\frac{\vartheta}{\vartheta_s}, \frac{N_{uo}}{N}, \frac{G_o}{S_u}, \Gamma(\gamma)\right) \tag{2}$$

in which N_{uo} is the ultimate vertical static force at the instant of bearing capacity failure $= (\pi + 2)S_u B$ for strip and $\approx 6.05 S_u \pi R^2$ for circular foundation; ϑ_S is a characteristic angle to be introduced below; $N_{uo}/N = \mathrm{F_s}$ is recognized as the static vertical factor of safety; G_o/S_u is the so-called "rigidity index"; and $\Gamma(\gamma; PI)$ is the shear modulus reduction curve. We utilize the $I_P = 30$ curve of Vucetic and Dobry (1991), as appropriate for the "typical" clay. Moreover, G_o/S_u has no effect on the function f as will be shown in the sequel, even if its value is varied parametrically between 800 (a value typical of a moderately-overconsolidated clay) and 200 (a lower bound often used in foundation analysis). Hence:

$$K_R \equiv K_R(\vartheta, N) = K_{R,elastic} \cdot f\left(\frac{\vartheta}{\vartheta_S}, F_S\right) \tag{3}$$

Figure 3 highlights the moment-rotation response of a footing for three values of F_s, the resulting secant rotational stiffness as a decreasing function of ϑ, and the snapshots of deformed meshes with the plastic deformation contours during the ultimate state.

Utilizing the results of a comprehensive numerical parameter study, for a variety of rectangular and a circular foundation plans, Gazetas et al. (2013) derived the following approximate relation:

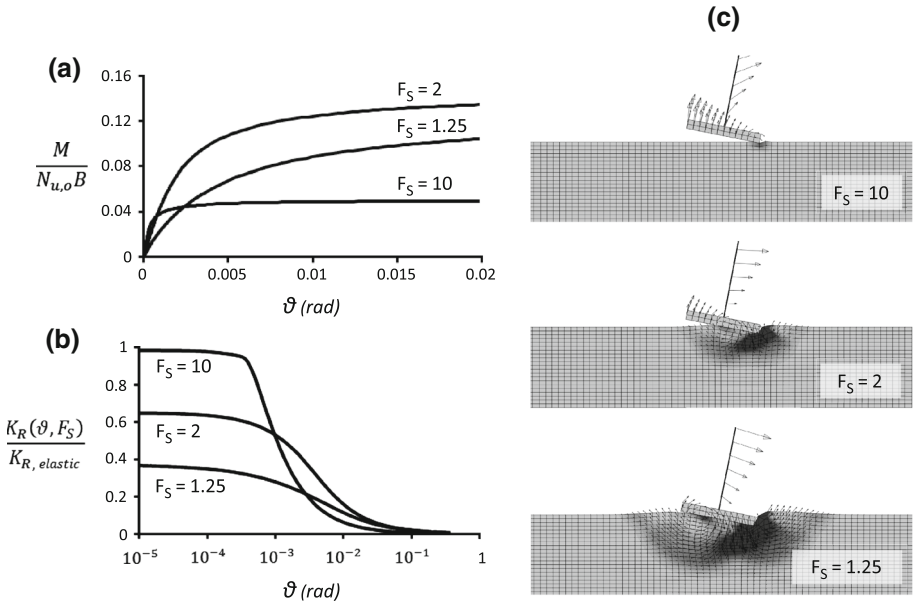

Fig. 3 Example of outcomes of rotational pushover on a strip footing for three static vertical safety factors: **a** dimensionless moment versus rotation; **b** normalized rotational stiffness versus rotation for three safety factors; **c** snapshots of deformed mesh at peak rotation, with superimposed movement *vectors* and *shading* for the (large) plastic strains

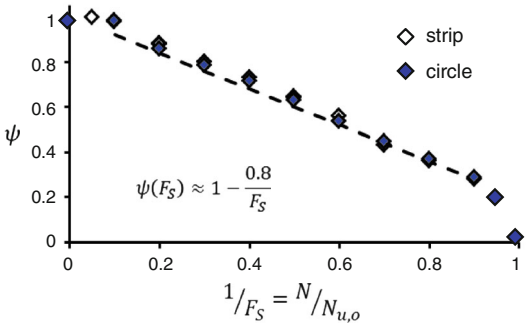

Fig. 4 The ψ as a unique function of the static factor of safety

$$K_R \approx K_{R,elastic} \cdot \psi\,(F_s) \cdot \chi\left(\frac{\vartheta}{\vartheta_S}, F_S\right) \tag{4}$$

in which:

- The purely-elastic stiffness is: for a strip footing of width B = 2b

$$K_{R,elastic} = \frac{\pi G b^2}{2\,(1-\upsilon)} \text{ (per unit length)} \tag{5}$$

  and for a circular footing of radius R

$$K_{R,elastic} = \frac{8GR^3}{3\,(1-\upsilon)} \tag{6}$$

- The function $\psi\,(F_s)$ accounts for the initial yielding of the soil under solely vertical forcing (i.e., before any moment is applied) and is plotted in Fig. 4. For both shapes:

$$\psi\,(F_s) \approx 1 - \frac{0.8}{Fs} \tag{7}$$

- The expression for the characteristic angle

$$\vartheta_s = \frac{NB}{4K_{R,elastic}\psi\,(F_s)}\left[1 - 0.22\left(1 - \frac{1}{F_s}\right)^2\left(\frac{B}{L}\right)^{0.2}\right] \tag{8}$$

  has been inspired by the analytical expression for the angle at which uplifting initiates in lightly-loaded foundations ($F_s > 10$); for all F_s values, however, the above expression for ϑ_s was derived by trial-and-error so that all the results plot within very narrow bands (Gazetas et al. 2013). Also, $B = 2b$ or $2R$ depending on footing shape
- Finally, the χ function is given graphically in Fig. 5 in terms of ϑ/ϑ_s, with the static F_s as a discretely-varying parameter.

As promised, we show in Fig. 6 that normalizing with ϑ_S eliminates the effect of the "rigidity index" G_o/S_u. Notice in the figure that as G_o/S_u increases uplifting takes place at smaller angles of rotation (due to increased soil stiffness), and hence the rapid decline of the secant stiffness with ϑ starts earlier. This obvious effect of G_o/S_u is well captured with a single curve after normalizing with ϑ_S expressed as in Eq. (8).

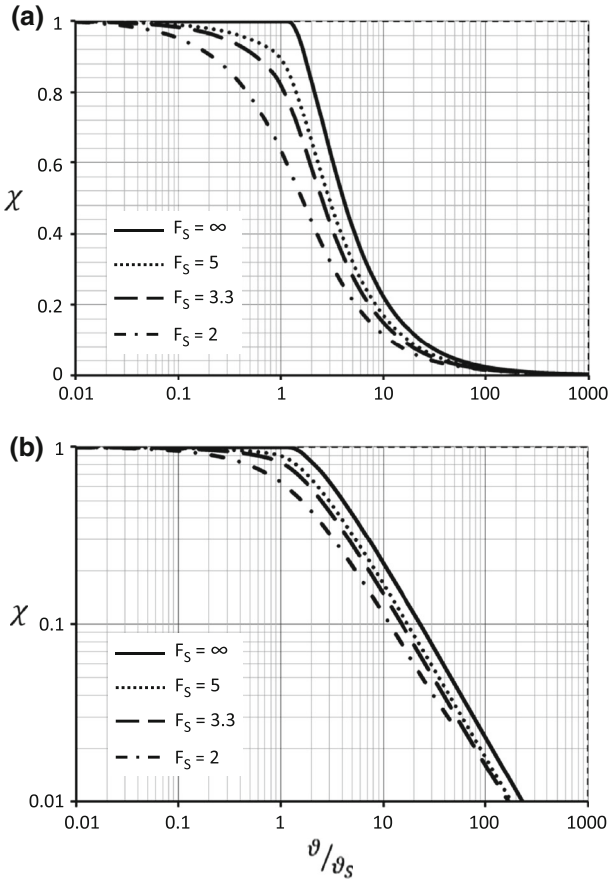

Fig. 5 Plot of the function backslash χ versus ϑ/ϑ_S and four values of F_s: **a** logarithmic and **b** bi-logarithmic plots (allowing focus on *small and large values* of ϑ/ϑ_S, respectively)

4.2 Frequency dependence

The rocking dynamic stiffness $\overline{K}_R$ is frequency dependent. For foundations bonded onto an elastic halfspace, $\overline{K}_R$ decreases with the normalized frequency $a_o = \omega R/V_s$ or $\omega\,\mathrm{b}/\mathrm{V_s}$ as shown in Fig. 7 for the two "extreme" values of Poisson's ratio (Luco and Westman 1971; Vetetsos and Wei 1971; Roesset 1975, 1980). The curves are not of course valid for uplifting foundations, let alone inelastic soil. Nevertheless, they can offer an approximation even in this case if the fundamental frequency of the rocking system is iteratively used for the ω value. Moreover, for seismic shaking of slender structures undergoing uplifting and mobilizing soil failure mechanisms, the effective frequencies are likely to be quite low, as will be elucidated in the sequel. Assuming

$$\overline{K}_R \approx K_R \tag{9}$$

is thus a reasonable approximation, consistent with the overall level of accuracy of the developed method.

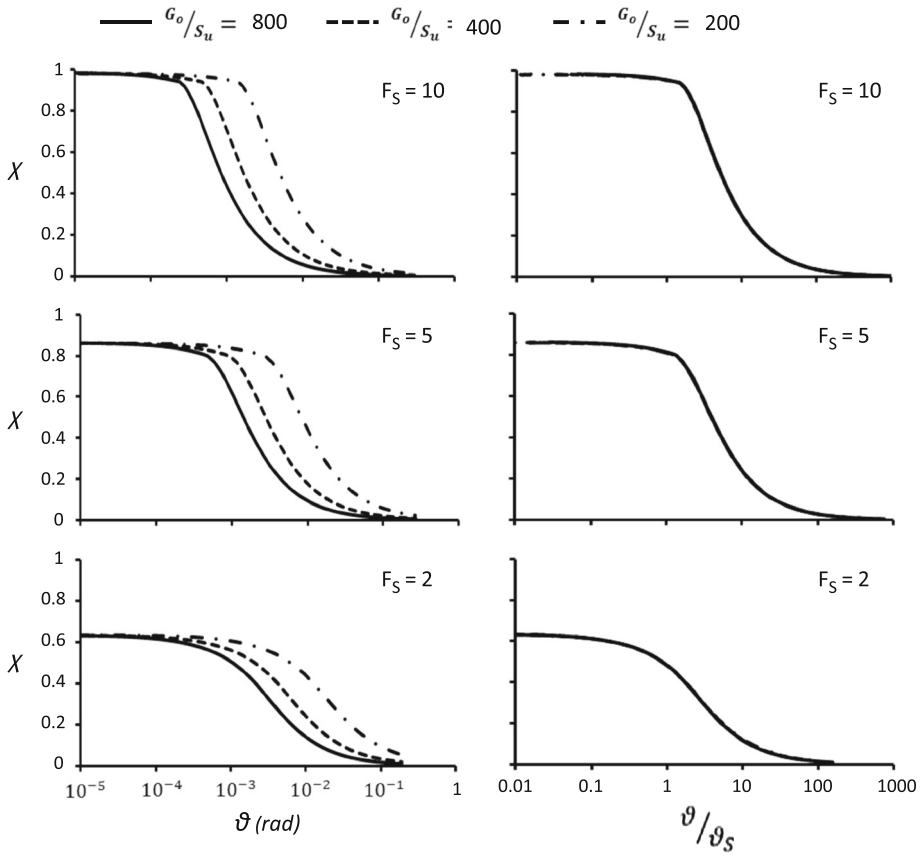

Fig. 6 The effect of "rigidity index" G_o/S_u is eliminated after normalizing the angle of rotation ϑ with the "characteristic" angle ϑ_s. Example for a circular footing and three factors of safety

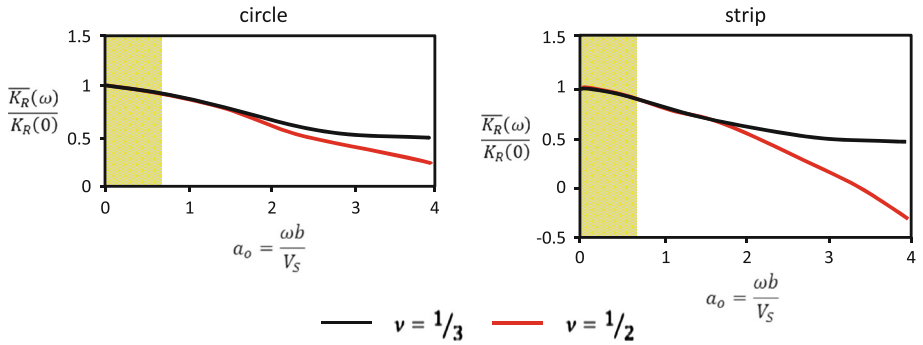

Fig. 7 Frequency dependence of the (dynamic) rocking stiffness of circular and strip foundations on elastic homogeneous halfspace

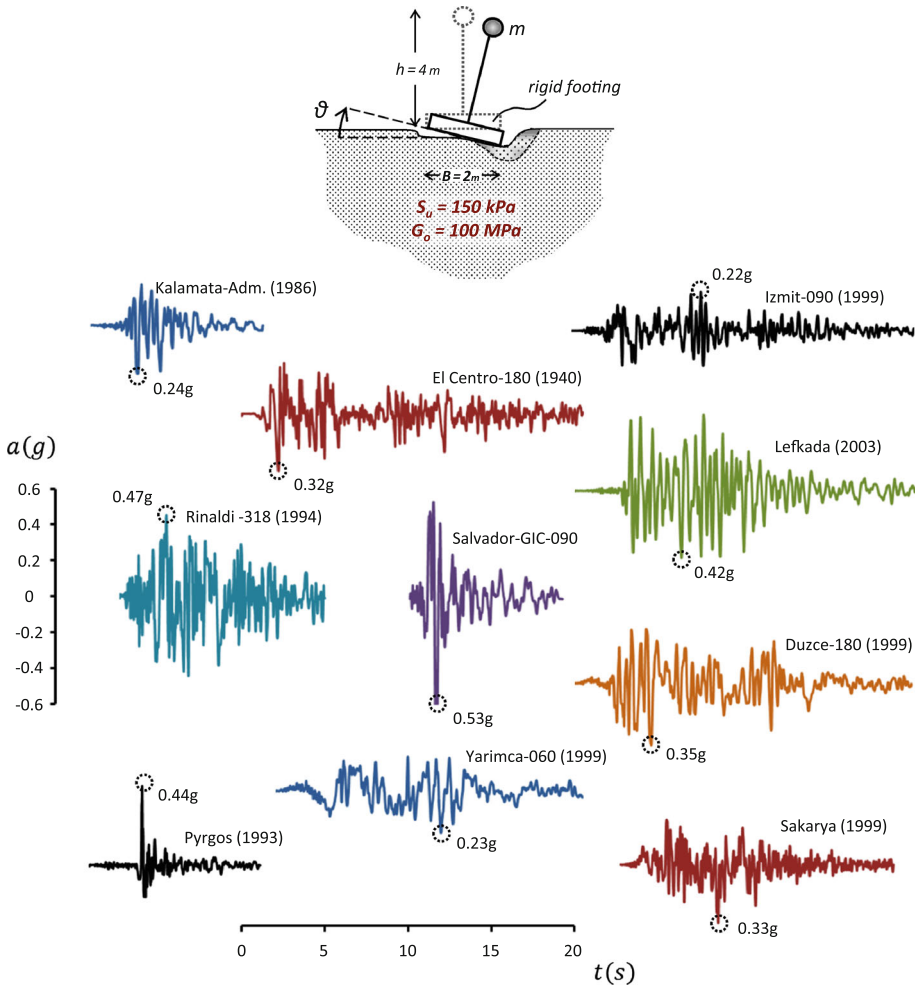

Fig. 8 Earthquake accelerograms used as excitation in the dynamic analyses

The effectiveness of the iterative "equivalent linear" approximation, is tested against the dynamic finite element analysis (properly modeling the soil). The comparison will also provide an indirect indication of the significance (if any) of the frequency dependence of $\overline{K}_R$.

To this end, the rigid oscillator pictured in Fig. 8 is subjected to 10 ground surface records, also shown in this figure. Parametrically varying the mass, three static factors of safety are obtained. The high slenderness ratio, $h/b = 4$, the variety in intensity, frequency-content, and duration of the used excitations, and the three values of F_s ensure that: (1) rocking is the dominant mode, and (2) small, moderate, and high nonlinearities will develop. From the overturning moment versus rotation loops of the finite element analysis the secant stiffness as a function of the angle of rotation is obtained (with reasonable accuracy). Normalizing by the factor $\psi(F_s) = 1 - 0.8/F_s$ and by the theoretical elastic rocking stiffness $K_R = (\pi/2)Gb^2/(1-\upsilon)$, "numerical" values of the dimensionless function $\chi(\vartheta/\vartheta_s, F_s)$

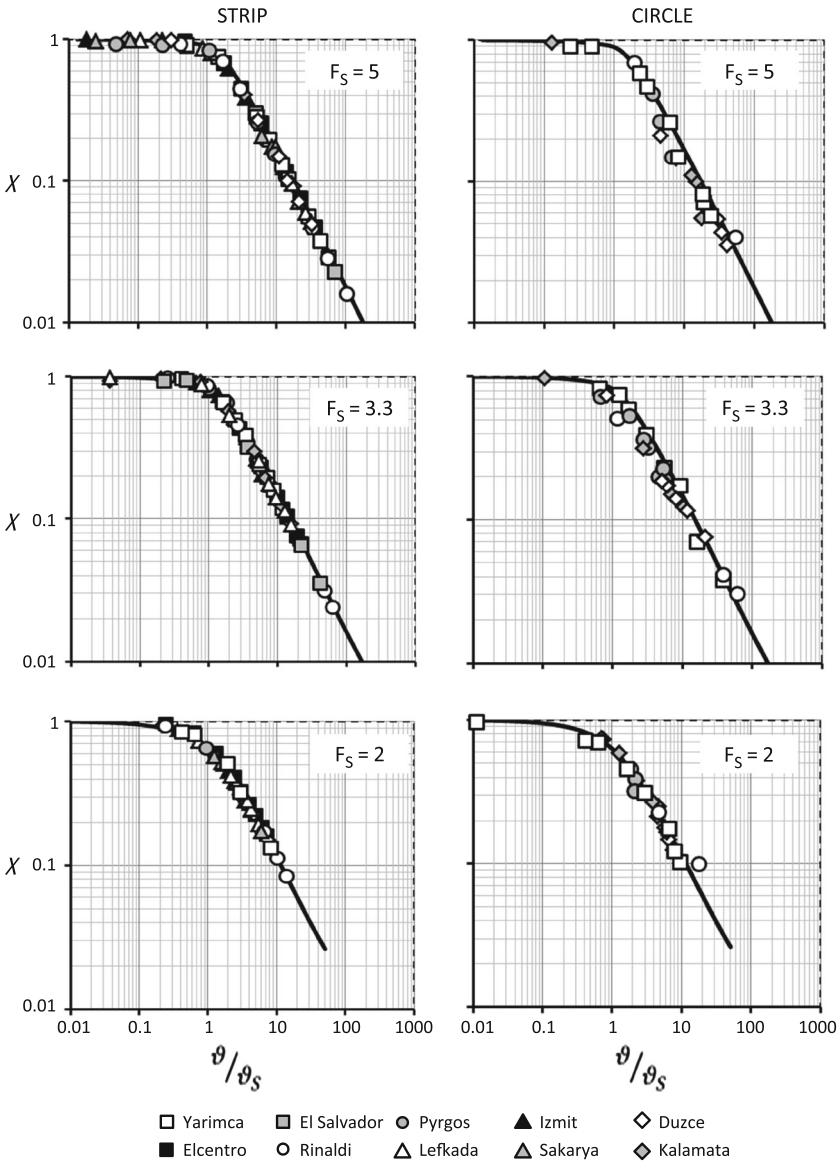

Fig. 9 Curves for $\chi(\vartheta/\vartheta_s, F_S)$: approximate (*black line*) versus finite-element (*points*)

are obtained. They are plotted in Fig. 9 as data points on top of the developed equivalent-linear curves of Fig. 5. Evidently, our approximations in deriving Fig. 5 and handling the frequency-dependence of stiffness lead to reasonably satisfactory results.

4.3 Effective natural period

The dynamic response of the above rigid oscillator is now utilized to further check the developed approximation for the rocking stiffness, but, moreover, to illustrate the role

of uplifting and/or soil inelasticity on the fundamental period of an oscillator $T_{R,nonlin}$. From the free-vibration part of the aforementioned "rigorous" dynamic analyses we obtain *estimates* of

$$T_{R,nonlin} = T_{R,nonlin}(\theta/\theta_{s,} F_s) \tag{10}$$

These estimates, plotted as data points in Fig. 10, are compared with the approximate theoretical solution to the governing free rocking oscillations

$$(mh^2)\ddot{\vartheta} + K_R\theta - mgh\,sin\theta \approx 0 \tag{11}$$

where the effective (equivalent-linear) K_R is obtained according to Eqs. 4–8. For relatively small values of ϑ, say $\vartheta < 2\vartheta_s$, the linearized approximation $sin\vartheta \approx \vartheta$ leads to

$$T_{R,nonlin} \approx 2\pi\sqrt{\frac{mh^2}{K_R - mgh}} \tag{12}$$

Note that the rigid superstructure has a zero fixed-base period; the periods in the graphs of Fig. 10 are the exclusive outcome of soil–structure interaction: nearly linear for $\vartheta < \vartheta_s$, and increasingly nonlinear as ϑ exceeds ϑ_s and F_s decreases from 5 to 2.

5 Equivalent damping (ξ_R)

Along with the equivalent-linear definition of the stiffness K_R as shown in Fig. 1c, an effective *hysteretic* damping factor $\xi_{R,h}$ can be obtained from the area of the corresponding hysteresis loop in a complete slow $M : \vartheta$ cycle. Such damping is solely due to the inelastic action in the soil. Under dynamic loading, however, two additional sources of damping are likely to appear:

(a) Radiation of waves which emanate at the footing-soil interface, spread outward, and thus carry energy away from the foundation.
(b) Impact of the footing onto the soil and concomitant vertical oscillatory motion, dissipate part of the kinetic energy imparted on the foundation.

5.1 Radiation damping ($\xi_{R,r}$)

For steady-state rocking oscillations on elastic soil radiation damping depends on frequency. At very low frequencies, wavelengths are large, and waves emanating from exactly opposite (with respect to the center) points of the soil-footing interface may easily "interfere destructively". Hence radiation of wave energy is hardly effective, and the associated damping is very small. In fact it is vanishingly small with ω tending to zero.

As if this were not enough, little if any radiation can take place below a cutoff frequency ω_c which depends on the stiffness and thickness of the soil stratum. Under elastic soil conditions (Kausel 1974; Kausel and Roesset 1975; Wolf 1988; Gazetas 1991):

$$\omega_c \approx \frac{1 \cdot 7}{(1 - v)}\frac{V_s}{H} \tag{13}$$

For the problem studied here radiation damping is further reduced by two additional phenomena:

- Uplifting of the footing, as a result of which the area of contact decreases and thus the emission of waves from the interface is reduced.

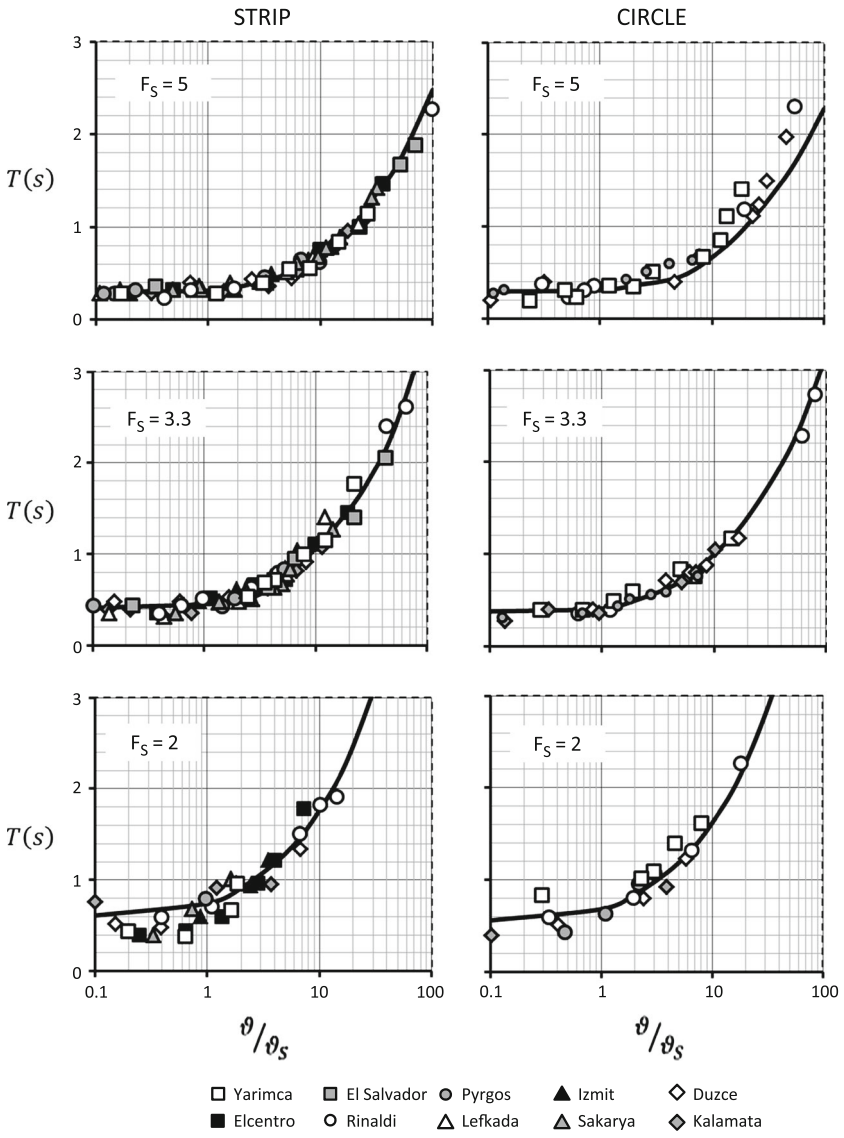

Fig. 10 Dominant period of rocking oscillations: equivalent-linear approximatel period (*black line*) versus period measured from the dynamic response time histories (*data points*)

- Inelasticity in the soil, as a result of which bearing-capacity failure mechanisms (and hence associated localized failure surfaces close to the footing) tend to develop, thereby creating a softer zone inside the (stiffer) soil; waves are trapped by multiple reflections within this zone, and radiation damping is further reduced if not eliminated.

Nevertheless, to obtain an upper-bound estimate of the radiation damping, purely linear analyses are performed with the finite-element models of Fig. 2b in which "infinite elements" are attached to the lateral boundaries of the static models to allow radiation. No material damping is introduced. A study is conducted with the distance L_m that defines the

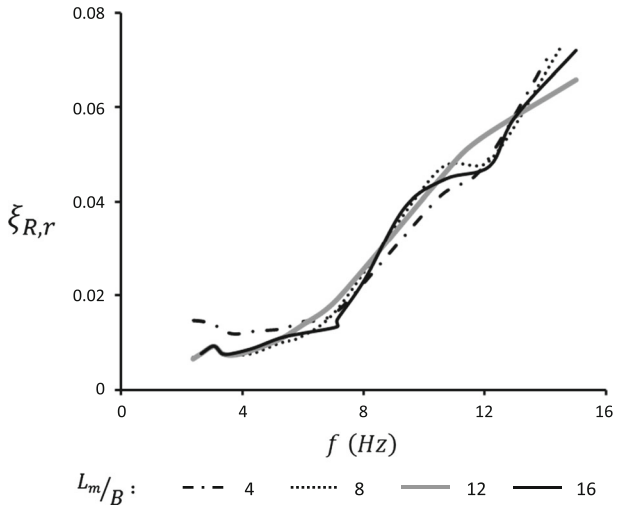

Fig. 11 Effect of distance between the "infinite" elements (Fig. 2): example for a strip footing of width B = 2 m, for elastic soil of depth H = 8 m, and low-strain Young's modulus E_o = 100 MPa

location of the "infinite elements", the shear wave velocity V_s, and the depth to rock H as parameters. The damping factor is determined approximately from the decay of free rocking vibrations.

The results are portrayed in Fig. 11 (effect of L_m) and Fig. 12 (effect of V_s and H). Figure 11 confirms that even a small L_m (only 4 times the footing width) leads to acceptable values at most frequencies. An interesting behavior is revealed in Fig. 12, in which nine combinations of H and V_s are considered. When $\xi_{R,r}$ is plotted versus the frequency of oscillation, both for a strip and a circle, three distinct curves appear, each representing a different shear velocity, regardless of the stratum thickness. Small fluctuations of all curves arise from the presence of the bedrock. As the soil becomes stiffer and V_s increases, damping ratio decreases for the same frequency. It is also worth noting that the rate at which $\xi_{R,r}$ increases with frequency is very small up to a specific frequency value (different for each V_s) implying the workings of an (imperfect) "cut off" frequency, below which damping ratio is negligible. Interestingly, when the abscissa, f, is normalized by V_s/H it yields three new distinct curves, one for each separate layer thickness H, regardless of the value of V_s !

All the results are collected in Fig. 13 in terms of both damping factor, $\xi_{R,r}$, and dashpot constant, $C_{R,r}$, as functions of $a_o = \omega b/V_s$ or $\omega R/V_s$ for strip or circle, respectively. Recall that $C_{R,r}$ is related to $\xi_{R,r}$ through the foundation stiffness and cyclic frequency:

$$C_{R,r} = 2K_R\xi_{R,r}/\omega \tag{14}$$

Figure 13 is nearly identical with rigorous steady-state analyses (Kausel 1974; Dobry and Gazetas 1986; Wolf 1988; Gazetas 1991; Dobry 2012). It can be used for estimating radiation damping using the natural frequency of the oscillator. With either choice, however, ω will rarely exceed $\omega_{max} \approx 2\pi/1 = 2\pi$ rad/s, since $T \approx 1$ s is a typical value of a slender elastic oscillator undergoing rocking accompanied with uplifting and strong inelasticity in the soil. Thus, even a very wide foundation with $B = 10$ m and $V_s \approx 250$ m/s (appropriate for our stiff clay) would lead to

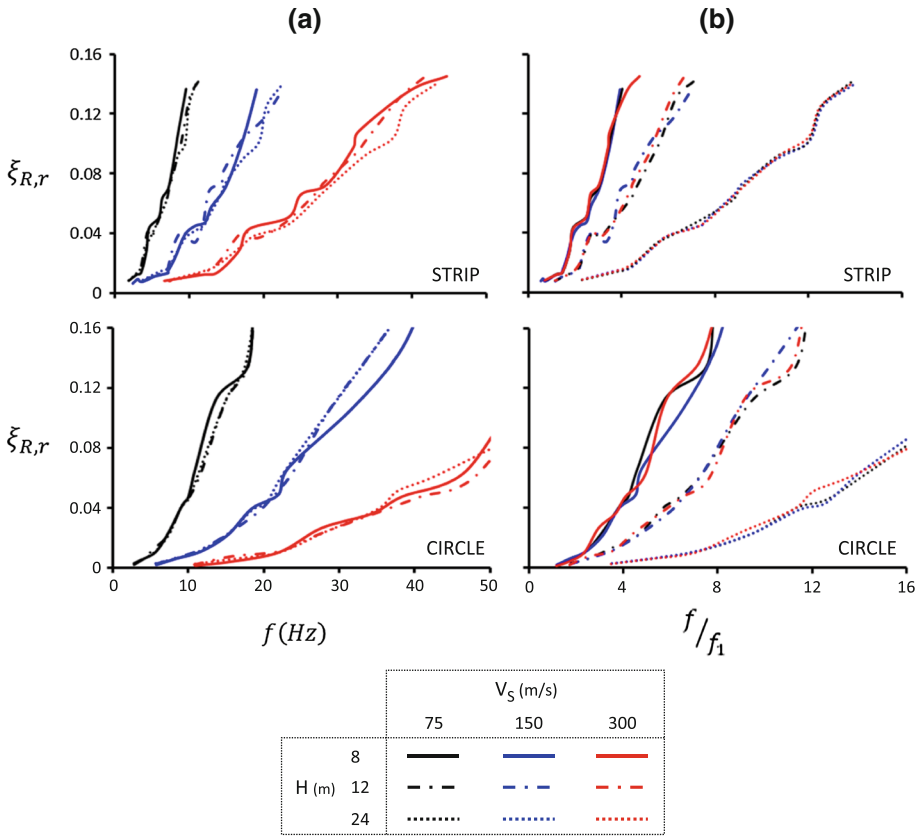

Fig. 12 Radiation damping for three stratum thicknesses, H, and three shear wave velocities, V_S : **a** damping factor versus frequency; **b** damping factor versus frequency divided with the fundamental natural frequency of the soil stratum in shear

$$a_{o,max} \sim (2\pi \times 10)/250 \approx 0.24 \tag{15}$$

From Fig. 13 it is seen that radiation damping would only rarely exceed a mere 2 %. Unsurprisingly, the 2-D strip foundation generates greater damping than its 3-D circular counterpart (recall the *"radiation damping paradox"*—Gazetas 1987; Wolf 1988).

5.2 Hysteretic damping($\xi_{R,h}$)

As already discussed, damping due to soil inelasticity would obviously increase with the amplitude of the angle of rotation, ϑ, and the magnitude of the static vertical force, N, carried by the foundation. It was obtained from the (slow) cyclic pushover loops in $M : \vartheta$ as explained in Fig. 1c.

Now, the normalized variables $F_s = N_{uo}/N$ and ϑ/ϑ_s uniquely define the value of the damping factor $\xi_{R,h}$ regardless of foundation shape, as depicted in Fig. 14. Notice the substantial values of $\xi_{R,h}$ for the heavily loaded foundation ($F_s = 2$), especially at values of the angle $\vartheta \approx 2\vartheta_s$ or larger.

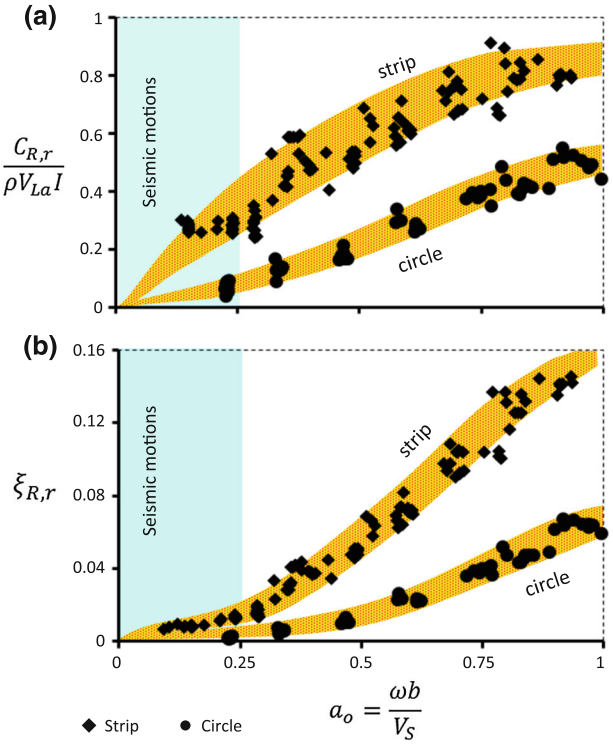

Fig. 13 Dimensionless plots for radiation damping, **a** normalized rotational dashpot coefficient C_r versus a_o; **b** damping ratio ξ versus a_o. The usual range of a_o for earthquakes and rocking is highlighted with *light grey*

5.3 Impact related damping ($\xi_{R,i}$)

In addition to energy dissipated in the soil due to its inelastic behavior and to energy carried away by propagating waves, an intensely rotating foundation may cause extra energy consumption due to the impacts that accompany its uplifting. The contribution, $\xi_{R,i}$, of this energy consumption to the damping factor, is expected to be significant when F_s is large and ϑ exceeds by far ϑ_s, since only then is uplifting significant. By contrast, at small values of F_s, say 2 or less, uplifting is hardly noticeable and $\xi_{R,i}$ is likely to be negligible.

Now, to understand the behavior for large values of F_s (say $F_s > 10$) and large values of ϑ (say $\vartheta > 3\vartheta_s$), let us consider rocking on a rigid base ($F_s \approx \infty$). Even a perfectly elastic impact generates energy loss for the structure due to changing of its angular velocity. From Makris and Roussos (2000) the angular velocity right after the impact is only a fraction of the one prior to impact:

$$\dot{\vartheta}^2(t_0^+) = r\dot{\theta}^2(t_0^-) \tag{16}$$

In which the fraction r is the so-called coefficient of restitution. If the momentum impulse principle is applied and energy loss due to interface mechanisms during impact is zero, the coefficient r for a rigid block of semi-height h and semi-width b is given by

$$r = \left(1 - \frac{3}{2} sin^2 \vartheta_c\right)^2, \quad \vartheta_c = arctan\,(b/h) \tag{17}$$

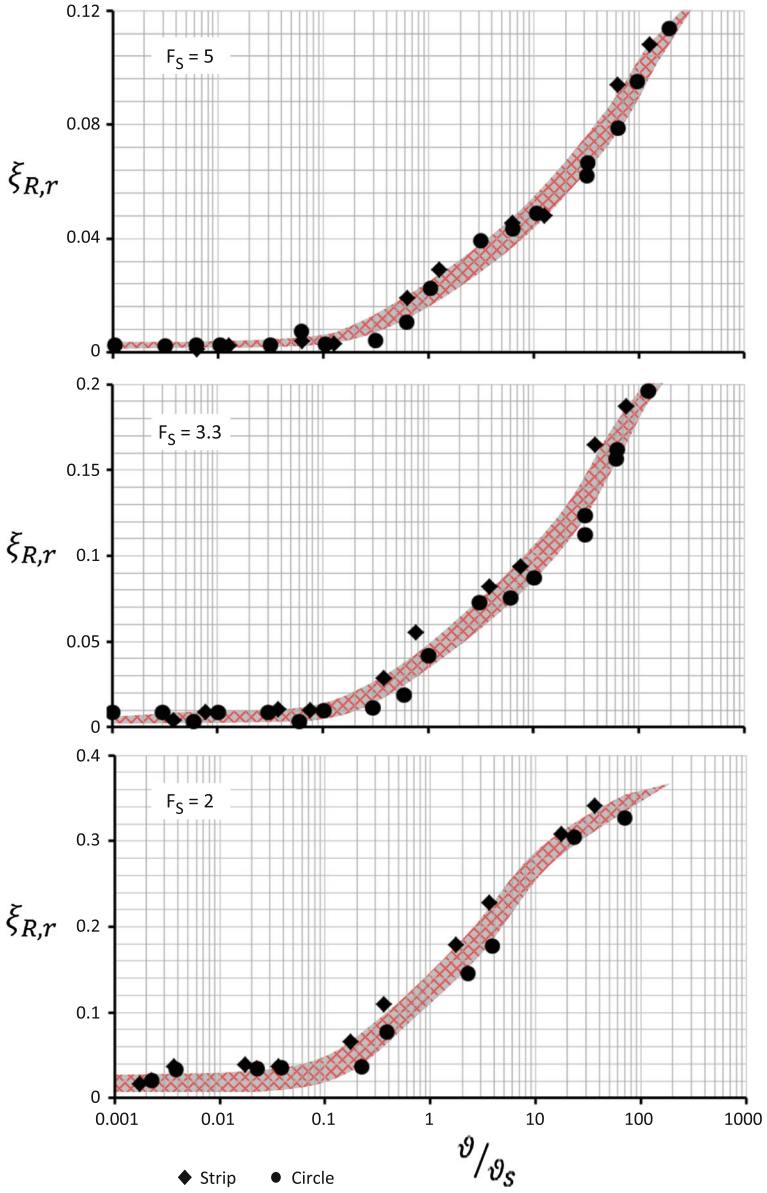

Fig. 14 Hysteretic damping factor: Results for strip and circular footings revealing the significance of the static factor of safety, F_S

Typical values of this (purely geometric) coefficient of restitution are in the range of 0.6–0.9 for a variety of slender structures (Markis and Zhang 2001; Apostolou et al. 2007). In reality of course the impact after a large rotation angle would hardly be elastic and some additional dissipation would accompany the impact. In any case, simultaneously with the substantial uplifting, the radiation damping may decrease as the area of wave emission is limited to the area of contact. This will reduce the net contribution of the impact to the overall damping.

To obtain a very *crude quantitative estimate* of $\xi_{R,i}$ we compare the pairs of loops of the $M:\vartheta$ curves obtained (1) under slow cyclic and (2) under dynamic loading. Impact occurs only in the dynamic case. Time-history finite-element ("rigorous") analyses are therefore performed with seismic excitation in the form of the records of Fig. 8. From these we obtain the (disproportionately large) areas of the dynamic loops compared to the quasi-static purely hysteretic loops. Hence

$$\boldsymbol{\xi_{R,h} + \xi_{R,i} \geq \xi_{R,h}} \tag{18}$$

where the subscripts h and i refer to hysteretic and impact damping, respectively. Figure 15 plots the left- and right-hand sides of Eq. 18. Fitted to the numerical data points (which admittedly were crudely estimated from the loops, despite the rigor of the analysis per se) are average curves of *the sum of hysteretic and impact damping*. For the reasons mentioned previously, they are considered as merely crude estimates of possible upper-bound curves. From the difference of the two set of curves in Fig. 15 the following *tentative* expression is given for the upper-bound damping originating from impact:

$$\Xi \approx 0.055 \left(1 + \frac{B}{L}\right) \left(1 - \frac{1}{F_S}\right)^2 \log\left(\frac{\vartheta}{\vartheta_S}\right) \tag{19}$$

in which B is the total width and L the total length of the foundation (for a strip $B/L = 0$; for a circle $B/L = 1$). To account for the simultaneous decrease of radiation damping (which is not reflected in Fig. 13) it is proposed that only a fraction, say 2/3, of the above Ξ value be used to obtain $\Xi_{R,i}$ Thus, finally

$$\xi_R \approx \xi_{R,h} + \xi_{R,r} + \xi_{R,i} \tag{20}$$

where $\xi_{R,h}$ and $\xi_{R,r}$ are obtained from the graphs of Figs. 13 and 14, respectively, while $\xi_{R,i} = (2/3)\Xi$, with Ξ given by Eq. 20.

6 Evaluation and limitations of the equivalent-linear approximation

An example elucidates the accuracy achieved using the developed K_R and ξ_R in an iterative equivalent-linear analysis of the system shown in Fig. 8, subjected to the 10 recorded ground motions at its base. The "rigorous" finite-element results are compared with those obtained by solving iteratively (and numerically) the differential equation:

$$(mh^2)\ddot{\vartheta} + C_R\dot{\vartheta} + K_R\vartheta - mgh\sin\vartheta = -mA(\mathrm{t})h\cos\vartheta \tag{21}$$

where K_R and C_R are obtained iteratively from the expressions and charts given in the paper, while the accelerogram $A(t)$ must be one corresponding to the ground surface.

The results of the two types of analysis are compared in Figs. 16, 17, 18. These figures aim at showing the *capabilities and limitations* of the developed approximations. Specifically:

(a) Figure 16 plots the time histories of the foundation angle of rotation and overturning moment for three iterations when the system of Fig. 8 is excited by the GIC record of the destructive San Salvador 1986 earthquake. In the three rows of M and ϑ plots, the "exact" finite-element curves do not change, since there is no iteration in that analysis (notice only the unavoidable change in the ordinate scale of the M curves). But of course there are three different equivalent-linear M and ϑ curves, each corresponding to one of the three iterations. In the first iteration we start with the elastic stiffness, $K_{R,elastic,}$ which produces a period of about 0.4 s (crude estimate "read" from the oscillatory motion, and

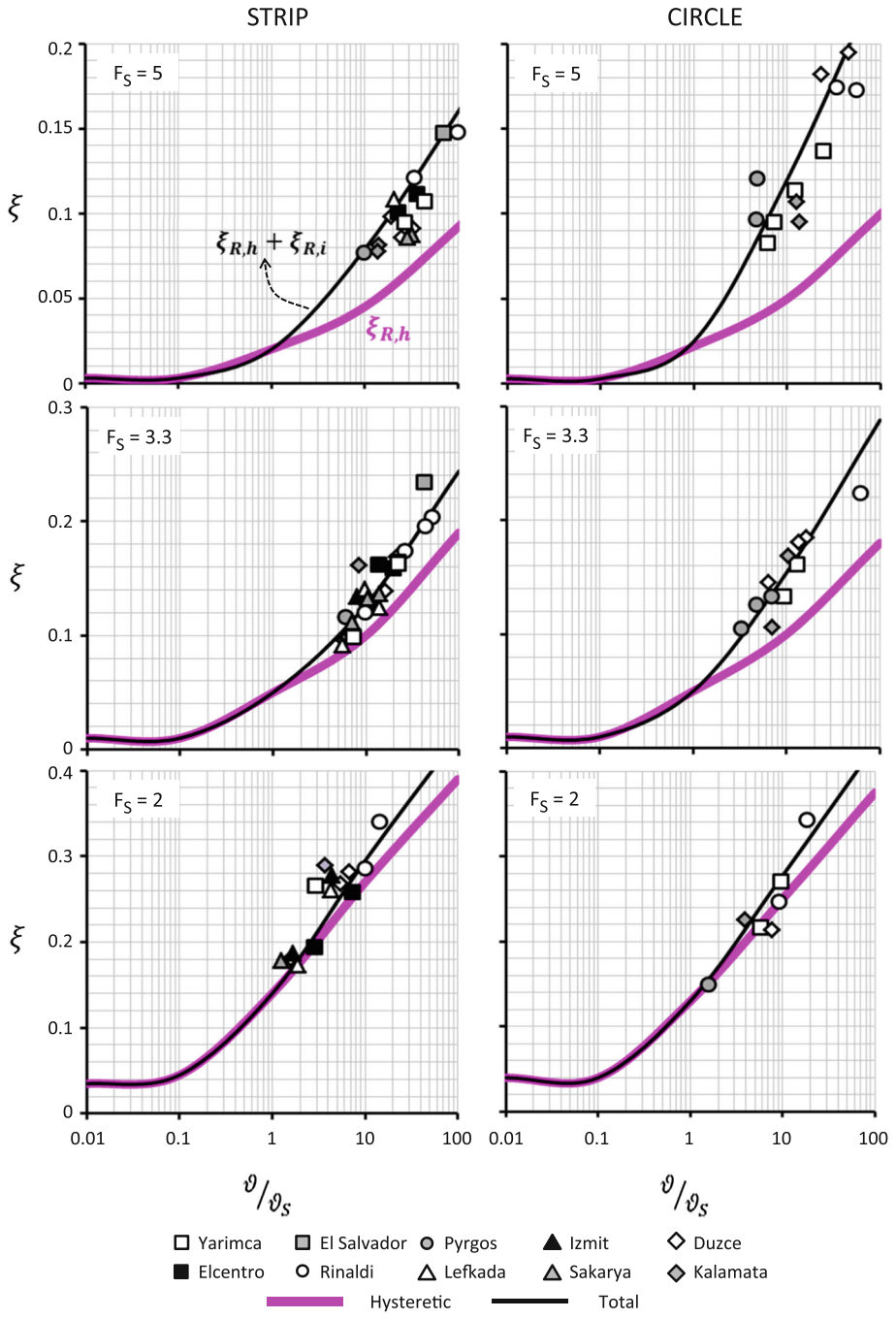

Fig. 15 The total damping exceeds the hysteretic one when $\theta > \theta_s$ due to impact and perhaps minor sliding

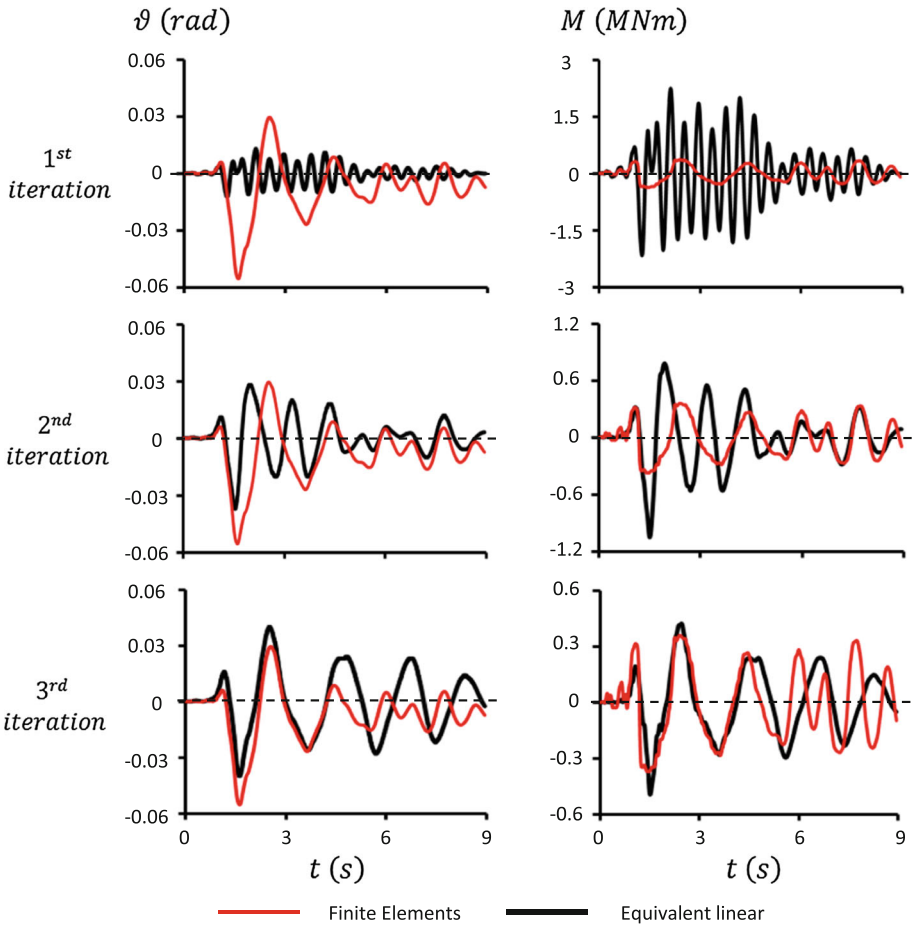

Fig. 16 Evaluation of the iterative equivalent-linear approximation for a strip footing. Factor of safety F_S 3.3, excitation: GIC record of the 1986 San Salvador earthquake. Time histories of rotation and moment for the equivalent linear are presented for three iterations

verified with Fig. 10). The outcome is an angle of rotation with a peak value, max ϑ, of about 0.01 rad—a large enough value to cause uplifting and inelasticity, as can be deduced from Figs. 3 and 6. No wonder the approximate results are completely different from the "exact" numerical solution.

Thus, for the second iteration the stiffness is much reduced leading to much larger period of oscillation, and hence to improved agreement with the "exact" finite-element analysis. The even larger angle of rotation (max $\vartheta \approx 0.3$ rad) leads to a further reduction in stiffness of the subsequent (third) iteration, and thereby to a further increase in period; the outcome is a very satisfactory third iteration, in which convergence has practically been almost achieved (max $\vartheta \approx 0.35$ rad).

(b) the comparison of the $M : \vartheta$ loops in Fig. 17 is by far the most severe test for the approximations and the iterative method. Being in essence a linear method it only aspires at capturing the amplitudes of response, not the detailed moment–rotation curves. Notice indeed that the equivalent-linear loops resemble in form of visco-elastic type curves,

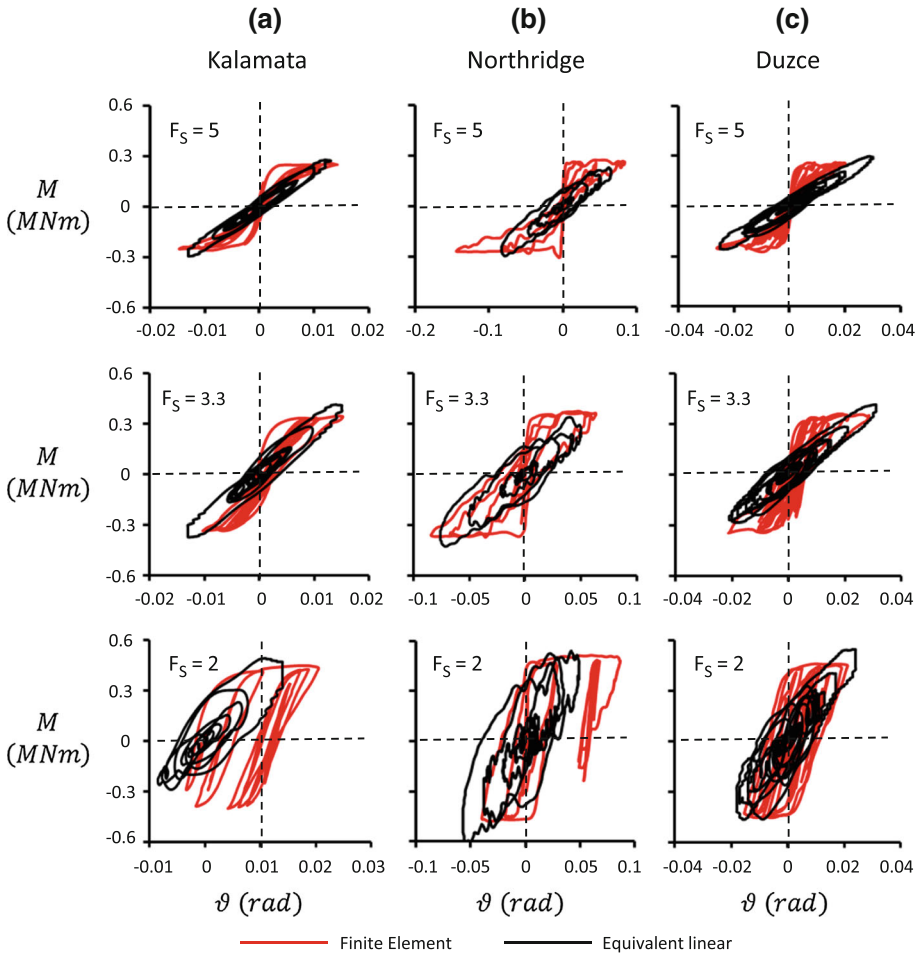

Fig. 17 Evaluation of the "equivalent linear" approximation for a strip footing: Moment-rotation loops are compared for three factors of safety and three accelerograms as excitation

rather than having the complicated "exact" shapes. This is hardly surprising, as it is a "designed" built-in drawback of the developed approximation.

Notwithstanding this limitation, the approximate $M : \vartheta$ curves come in general very close to the extremes of the "exact" loops, while the areas of the largest approximate loops seem (by naked eye) to be fairly similar with the corresponding areas of the "exact" loops.

(c) Figure 18 further demonstrates the satisfactory prediction of the peak values of the angle of rotation. Although admittedly on a doubly logarithmic scale, it is seen that on average "exact" and approximate methods lead to angles differing by not more than 20 % (with few exceptions).

7 Conclusion

For the problem of nonlinear and inelastic rocking vibrations of shallow strip and circular foundations, the paper has developed simplified expressions and dimensionless charts to

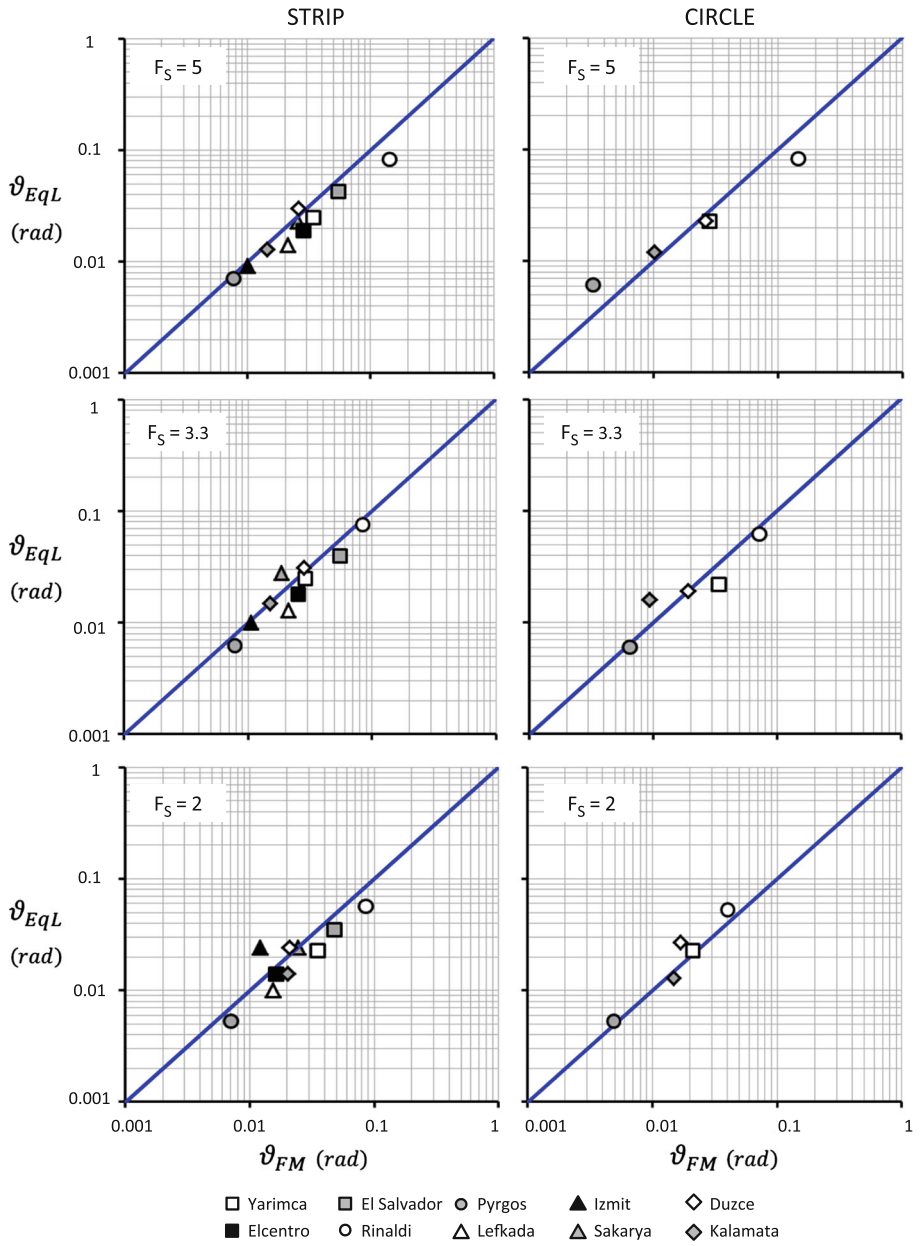

Fig. 18 Comparison of the peak angle of rotation calculated with the "equivalent linear" approximation (ϑ_{EqL}) and finite elements (ϑ_{FM})

obtain the equivalent-linear secant stiffness and effective damping. This was accomplished by utilizing the results of an extensive parametric finite-element study treating them as numerical experiments which were "fed" into our physically-simplified conceptual models. Extensive comparisons have shown that even intense vibrations, entailing significant uplifting of the

footing from the supporting ground and strong inelastic response of the soil, can be described with sufficient realism with the developed approximation, without of course capturing the complicated details of the numerical solution.

Acknowledgments The financial support of this work has been provided through the European Research Council (ERC) Program "Ideas: Support of Frontier Research", under Contract number ERC–2008–AdG–228254–DARE. We are thankful for this support. Evangelia Garini's help in the preparation of the figures is greatly appreciated, as are the constructive detailed comments by the reviewers.

References

Abate G, Massimino MR, Maugeri M, Muir Wood D (2010) Numerical modeling of a shaking table test for soil-foundation-superstructure interaction by means of a soil constitutive model implemented in a FEM code. Geotech Geol Eng 28:37–59

Allotey N, El Naggar MH (2003) Analytical moment-rotation curves for rigid foundations based on Winkler model. Soil Dyn Earthq Eng 23:367–381

Anastasopoulos I (2010) Beyond conventional capacity design: towards a new design philosophy. In: Orense RO, Chow N, Pender MJ (eds) Soil-foundation-structure interaction. CRC Press, New York, pp 213–220

Anastasopoulos I, Gazetas G, Loli M, Apostolou M, Gerolymos N (2010) Soil failure can be used for seismic protection of structures. Bull Earthq Eng 8:309–326

Apostolou M, Gazetas G, Garini E (2007) Seismic response of slender rigid structures with foundation uplifting. Soil Dyn Earthq Eng 27:642–654

Apostolou M (2011) Soil–structure interaction under strong seismic moment: material and geometric nonlinearity. PhD Thesis. National Technical University of Athens, Greece

Chatzigogos CT, Pecker A, Salencon J (2009) Macroelement modeling of shallow foundations. Soil Dyn Earthq Eng 29(6):765–781

Chen XC, Lai YM (2003) Seismic response of bridge piers on elastic-plastic Winkler foundation allowed to uplift. J Sound Vib 266(5):957–965

Cremer C, Pecker A, Davenne L (2002) Modeling of nonlinear dynamic behavior of a shallow strip foundation with macro-element. J Earthq Eng 6(2):175–211

Dobry R, Gazetas G (1986) Dynamic response of arbitrarily-shaped foundations. J Geotech Eng ASCE 113(2):109–135

Dobry R (2012) Simplified methods in soil dynamics. In: 21st Nabor Carrillo Lecture, Sociedad Mexicana de Ingenieria Geotecnica, Mexico, pp 1–47

Faccioli E, Paolucci R, Vanini M (1998) 3D site effects and soil-foundation interaction in earthquake and vibration risk evaluation. Report of the European research project TRISEE, Politecnico di Milano

Figini R (2010) Nonlinear dynamic soil–structure interaction: application to seismic analysis of structures on shallow foundations. Doctoral Disertation, Politecnico di Milano

Gajan S, Phalen JD, Kutter BL, Hutchinson TC, Martin G (2005) Centrifuge modeling of load-deformation behavior of rocking shallow foundations. Soil Dyn Earthq Eng 25:773–783

Gajan S, Kutter BL (2008) Capacity, settlement and energy dissipation of shallow footings subjected to rocking. Geotech Geoenviron Eng 134:1129–1141

Gazetas G (1987) Simple physical methods for foundation impedances. In: Benerjee PK, Butterfield R (eds) Dynamics of foundations and buried structures. Elsevier Applied Science, Chapter 2, pp 44–90

Gazetas G (1991) Formulas and charts for impedances of surface and embedded foundations. J Geotech Eng ASCE 117(9):1129–1141

Gazetas G, Apostolou M (2004) Nonlinear soil–structure interaction: foundation uplifting and soil yielding. In: Celebi M (ed) Proceedings of the 3rd USA–Japan workshop on soil–structure interaction. Menlo Park

Gazetas G, Anastasopoulos I, Adamidis O, Kontoroupi T (2013) Nonlinear rocking stiffness of foundations. Soil Dyn Earthq Eng 47:83–91

Gelagoti F, Kourkoulis R, Anastasopoulos I, Gazetas G (2012) Rocking isolation of frame structures founded on separate footings. Earthq Eng Struct Dyn 41:1177–1197

Gerolymos N, Apostolou M, Gazetas G (2005) Neural network analysis of overturning response under near-fault type excitation. Earthq Eng Eng Vib Springer 4(2):213–228

Gerolymos N, Gazetas G (2006) Development of Winkler model for static and dynamic response of caisson foundations with soil and interface nonlinearities. Soil Dyn Earthq Eng 26(5):363–376

Harden CW, Hutchinson TC, Moore M (2006) Investigation into the effects of foundation uplift on simplified seismic design procedures. Earthq Spectra 22(3):663–692
Houlsby GT, Cassidy MJ, Einav I (2005) A generalized Winkler model for the behavior of shallow foundation. Géotechnique 55(6):449–460
Housner GW (1963) The behavior of inverted pendulum structures during earthquakes. Bull Seismol Soc Am 53(2):403–417
Kausel E (1974) Forced vibrations of circular foundations on layered media. Research Report R74–11. Department of Civil Engineering, Massachusetts Institute of Technology
Kausel E, Roesset JM (1975) Dynamic stiffness of circular foundations. J Eng Mech Div ASCE 101:771–785
Kawashima K, Nagai T, Sakellaraki D (2007) Rocking seismic isolation of bridges supported by spread foundations. In: Proceedings of 2nd Japan-Greece workshop on seismic design, observation, and Retrofit of foundations. Japanese Society of Civil Engineers, Tokyo, pp 254–265
Koh AS, Spanos P, Roesset JM (1986) Harmonic rocking of rigid block on flexible foundation. J Eng Mech ASCE 112(11):1165–1180
Kourkoulis R, Anastasopoulos I, Gelagoti F, Kokkali P (2012) Dimensional analysis of SDOF systems rocking on inelastic soil. J Earthq Eng 16(7):995–1022
Kutter BL, Martin G, Hutchinson TC, Harden C, Gajan S, Phalen JD (2003) Workshop on modeling of nonlinear cyclic load-deformation behavior of shallow foundations. Report of PEER Workshop. University of California, Davis
Luco JE, Westman RA (1971) Dynamic response of circular footings. J Eng Mech Div ASCE 97(5):1381–1395
Makris N, Roussos Y (2000) Rocking response of rigid blocks under near source ground motions. Géotechnique 50(3):243–262
Markis N, Zhang J (2001) Rocking response and overturning of anchored blocks under pulse-type motions. J Eng Mech ASCE 127(5):484–493
Martin G.R., Lam P (2000) Earthquake resistant design of foundations: retrofit of existing foundations. In: Proceedings of the geo-engineering 2000 conference, Melbourne, Australia, state-of-the art paper
Massimino MR, Maugeri M (2013) Physical modeling of shaking table tests on dynamic soil-foundation interaction and numerical and analytical simulation. Soil Dyn Earthq Eng J 49:1–18
Meek J (1975) Effect of foundation tipping on dynamic response. J Struct Div ASCE 101(7):1297–1311
Palmer AC (2008) Dimensional analysis and intelligent experimentation. Would Scientific Publishing, Singapore
Panagiotidou AI (2010) 2D and 3D inelastic seismic response analysis of foundation with uplifting and $P-\Delta$ effects. Diploma thesis, National Technical University, Athens
Panagiotidou AI, Gazetas G, Gerolymos N (2012) Pushover and seismic response of foundations on stiff clay: analysis with P $-\Delta$ effects. Earthq Spectra 28(4):1589–1618
Paolucci R (1997) Simplified evaluation of earthquake induced permanent displacement of shallow foundations. J Earthq Eng 1(3):563–579
Paolucci R, Pecker A (1997) Seismic bearing capacity of shallow strip foundations on dry soils. Soils Found 37:95–105
Paolucci R, Shirato M, Yilmaz MT (2008) Seismic behavior of shallow foundations shaking table experiments vs numerical modeling. Earthq Eng Struct Dyn 37:577–595
Paolucci R, Figini R, Petrini L (2013) Introducing dynamic non-linear soil-foundation-structure interaction effects in displacement-based seismic design. Earthq Spectra 29
Pecker A (2011) Influence of nonlinear soil structure interaction on the seismic demand of bridges. In: Proceedings of the international conference on innovations on bridges and soil bridge interaction. Evgenides Foundation Publications, Athens, pp 91–106
Pitilakis D, Dietz M, Clouteau D, Modaressi A (2008) Numerical simulation of dynamic soil–structure interaction in shaking table testing. Soil Dyn Earthq Eng 28:453–467
Roesset JM (1980) Stiffness and damping coefficients of foundations. In: Dobry R, O'Neil MW (eds) Dynamic response of foundations: analytical aspects. ASCE, pp 1–30
Roesset JM (1975) The use of simple models in soil–structure interaction. Civil Eng Nucl Power ASCE 1:1–25
Vetetsos AS, Wei YT (1971) Lateral and rocking vibration of footings. J Soil Mech Found Div ASCE 97:1227–1248
Vucetic M, Dobry R (1991) Effect of soil plasticity on cyclic response. J Geotech Eng ASCE 117(1):89–107
Wolf JP (1988) Soil–structure interaction analysis in time-domain. Prentice-Hall, Englewood Cliffs, NJ
Zhang J, Makris N (2001) Rocking response and overturning of free-standing blocks under cycloidal pulses. J Eng Mech ASCE 127(5):473–483